Title

The effect of sevoflurane exposure on cell-type-specific changes in the prefrontal cortex in young mice.

Authors

Zhao, Bao-Jian

Song, Shao-Yong

Zhao, Wei-Ming

et al.

Publication Date

2024-02-01

DOI

10.1111/jnc.16068

Received: 25 September 2023 | Revised: 29 December 2023 | Accepted: 18 January 2024

DOI: 10.1111/jnc.16068

Journal of Neurochemistry JNC The Official Journal of the International Society for Neurochemistry WILEY

ORIGINAL ARTICLE

The effect of sevoflurane exposure on cell-type-specific changes in the prefrontal cortex in young mice

Bao-Jian Zhao[1,2,3] | Shao-Yong Song[1,2,4] | Wei-Ming Zhao[1,2] | Han-Bing Xu[1,2] | Ke Peng[1,2] | Xi-Sheng Shan[1,2] | Qing-Cai Chen[1,2] | Hong Liu[5] | Hua-Yue Liu[1,2,6] | Fu-Hai Ji[1,2]

[1]Department of Anesthesiology, First Affiliated Hospital of Soochow University, Suzhou, Jiangsu, China

[2]Institute of Anesthesiology, Soochow University, Suzhou, Jiangsu, China

[3]Department of Anesthesiology, Nanjing Stomatological Hospital, Affiliated Hospital of Medical School, Nanjing University, Nanjing, Jiangsu, China

[4]Department of Pain Medicine, Dushu Lake Hospital Affiliated of Soochow University, Suzhou, Jiangsu, China

[5]Department of Anesthesiology and Pain Medicine, University of California Davis Health, Sacramento, California, USA

[6]Ambulatory Surgery Center, First Affiliated Hospital of Soochow University, Suzhou, Jiangsu, China

Correspondence
Hua-Yue Liu and Fu-Hai Ji, Department of Anesthesiology, First Affiliated Hospital of Soochow University, Suzhou, Jiangsu 215006, China.
Email: docliu.hy@163.com; jifuhaisuda@163.com

Funding information
Suzhou Clinical Medical Center for Anaesthesiology, Grant/Award Number: Szlcyxzxj202102; Six Talent Peaks Project in Jiangsu Province, Grant/Award Number: WSN-022; Suzhou Medical Health Science and Technology Innovation Project, Grant/Award Number: SKY2022136; Jiangsu Medical Association Anaesthesia Research Project, Grant/Award Number: SYH-32021-0036 (2021031); Key Medical Research Projects in Jiangsu Province, Grant/Award Number: ZD2022021; National Natural Science Foundation of China, Grant/Award Number: 82001126 and 82072130; Gusu Health Talent Project of Soochow, Grant/Award Number: GSWS2021062

Abstract

Sevoflurane, the predominant pediatric anesthetic, has been linked to neurotoxicity in young mice, although the underlying mechanisms remain unclear. This study focuses on investigating the impact of neonatal sevoflurane exposure on cell-type-specific alterations in the prefrontal cortex (PFC) of young mice. Neonatal mice were subjected to either control treatment (60% oxygen balanced with nitrogen) or sevoflurane anesthesia (3% sevoflurane in 60% oxygen balanced with nitrogen) for 2 hours on postnatal days (PNDs) 6, 8, and 10. Behavioral tests and single-nucleus RNA sequencing (snRNA-seq) of the PFC were conducted from PNDs 31 to 37. Mechanistic exploration included clustering analysis, identification of differentially expressed genes (DEGs), enrichment analyses, single-cell trajectory analysis, and genome-wide association studies (GWAS). Sevoflurane anesthesia resulted in sociability and cognition impairments in mice. Novel specific marker genes identified 8 distinct cell types in the PFC. Most DEGs between the control and sevoflurane groups were unique to specific cell types. Re-defining 15 glutamatergic neuron subclusters based on layer identity revealed their altered expression profiles. Notably, sevoflurane disrupted the trajectory from oligodendrocyte precursor cells (OPCs) to oligodendrocytes (OLs). Validation of

Abbreviations: ADHD, attention-deficit/hyperactivity disorder; DEGs, differentially expressed genes; FDR, false discovery rate; GEMs, Gel Bead-In-Emulsions; GO, gene ontology; GWAS, genome-wide association studies; ISH, in situ hybridization; KEGG, Kyoto Encyclopedia of Genes and Genomes; MAST, model-based analysis of single-cell transcriptomics; NCBI, National Center for Biotechnology Information; OLs, oligodendrocytes; OPCs, oligodendrocyte precursor cells; PCR, polymerase chain reaction; PFC, prefrontal cortex; PND, postnatal day; RRID, Include Research Resource Identifier; SD, standard deviation; SLM, smart local moving; snRNA-seq, single-nucleus RNA sequencing; SRA, Sequence Read Archive; STAR, Spliced Transcripts Alignment to a Reference; t-SNE, t-distributed stochastic neighbor embedding; UMAP, Uniform Manifold Approximation and Projection; UMI, unique molecular identifier.

Bao-Jian Zhao, Shao-Yong Song and Wei-Ming Zhao contributed equally to this work.

disease-relevant candidate genes across the main cell types demonstrated their association with social dysfunction and working memory impairment. Behavioral results and snRNA-seq collectively elucidated the cellular atlas in the PFC of young male mice, providing a foundation for further mechanistic studies on developmental neurotoxicity induced by anesthesia.

KEYWORDS
developmental sevoflurane neurotoxicity, prefrontal cortex, single-nucleus RNA sequencing

1 | INTRODUCTION

Approximately 1 in 7 children in the United States undergo general anesthesia and surgical procedures before the age of 3, with 25% experiencing repeated or prolonged exposure to anesthetics (Rabbitts et al., 2010; Shi et al., 2018). The Food and Drug Administration's "Drug Safety Communication" in December 2016 (https://www.fda.gov/drugs/drug-safety-and-availability) highlighted potential impacts on brain development from such exposure. A recent randomized study found no neurodevelopmental outcomes at age 5 following a single episode of general anesthesia for approximately 1 hour in infants (McCann et al., 2019). However, the Mayo Anesthesia Safety in Kids study indicated associations between multiple exposures to general anesthesia and surgery before age 3 and neuropsychological domains, including motor skills, processing speed, executive function, behavior, and reading (Warner et al., 2018).

Sevoflurane, commonly used for pediatric surgeries, has been implicated in neurotoxicity in various brain regions with multiple neonatal exposures (Sun et al., 2022). The prefrontal cortex (PFC), a region vulnerable to anesthetic-induced developmental neurotoxicity, plays a crucial role in cognitive functions such as social behavior, working memory, decision-making, and fine motor skills (Cheng et al., 2022). Additionally, the PFC exhibits neuroplasticity during postnatal life, potentially contributing to neurotoxicity and neuropsychiatric disorders (Miller et al., 2002). Studies have linked multiple sevoflurane exposures to disruptions in fine motor control skills and cognitive functions in the PFC, including mRNA methylation regulation (Zhang et al., 2022) and oligodendrocyte maturation impairment (Wu et al., 2020).

To address the gaps in understanding sevoflurane-induced neurotoxicity, this study utilized behavioral tests and single-nucleus RNA sequencing (snRNA-seq) to categorize neuron and non-neuronal cell subtypes in the mouse PFC. The investigation aimed to unveil distinct transcriptional dynamics in response to clinically significant concentrations of sevoflurane. Special attention was given to the risk variants of neuropsychiatric disease-relevant genes, particularly those associated with social interaction disorder, using cell-type-specific differentially expressed genes identified through genome-wide association studies (GWAS). This snRNA-seq study explored the potential pathogenesis of sevoflurane-induced neurotoxicity by examining individual PFC cells, providing a comprehensive cellular atlas under both physiological and pathological conditions. These insights lay a foundation for a better understanding of PFC's role in sevoflurane-induced neurotoxicity.

2 | MATERIALS AND METHODS

2.1 | Animals and experiments

The animal study protocol (NO. 202207A0502) received approval from the Ethics Committee of Soochow (Suzhou, China) and adhered to the Laboratory Animal Management Committee of China's guidelines. C57BL/6J mice (RRID:MGI:7264769) were procured from Slaccas Laboratory (Shanghai, China). Mice offspring, along with littermates (4–8 pups) and respective mothers, were housed in individual, ventilated cages within a specific pathogen-free room under a 12-h light/dark cycle at 22–24°C, with ad libitum access to food and water. Sequential numbers were assigned to pups using ear tags.

Mice were randomly assigned to the control or sevoflurane group using an online tool (https://www.randomizer.org/). The animal model made by principal investigator, as detailed in a previous study (Song, Peng, et al., 2023; Song, Zhao, et al., 2023), involved male or female offspring exposed to either the sevoflurane or the control condition for 3 non-consecutive days (on postnatal days 6, 8, and 10) from 9:00 am to 11:00 am, without blinding investigators. The sevoflurane group received 3% sevoflurane plus 60% oxygen (balanced with nitrogen) for 2 h using the Datex-Ohmeda anesthesia system (Madison, WI, USA). Sevoflurane and oxygen concentrations were continuously monitored with a Vamos gas analyzer (Dräger Medical, Germany). Rectal temperature was maintained at 37 ± 0.5°C in the chamber. The control group received 60% oxygen balanced with nitrogen for 2 h. Following anesthesia, mice were returned to home cages under standard care.

Our previous study demonstrated that exposure to 3% sevoflurane, compared to the control group, did not alter pH values, partial pressures of oxygen, partial pressures of carbon dioxide, electrolytes, or hematocrit levels (Song et al., 2019).

2.2 | Behavioral tests

Behavioral assessments were conducted on male and female mice weighing 20–23 g from postnatal days (PNDs) 31–37, as previously

outlined (Sun et al., 2022). Male and female mice were allowed a 1-h acclimation period in the testing environment before the commencement of each behavioral test. All behavioral tests were performed and analyzed in a blinded manner. The experimenters were unaware of study groups during behavioral tests and data analysis. Allocation details were securely stored in an opaque sealed envelope, ensuring experimenter blinding until the final analysis.

2.2.1 | Open field test

Mice were gently placed in a corner of a chamber (40×40×30 cm), and their movements were recorded over 10 min using an overhead camera in conjunction with the ANY-maze system for tracking (RRID:SCR_014289). Parameters, including total distance moved, movement speed, time spent in the center, and entries into the center (20×20 cm), were accurately documented.

2.2.2 | Elevated plus maze

The apparatus featured two closed arms (30×6×15 cm) and two open arms (30×6×15 cm), elevated 60 cm above the floor. Each mouse was initially placed in the center of the maze, facing an open arm, and allowed to explore the maze for 5 min. Entries into the open arms (all four paws) and time spent in the open arms were precisely calculated using the ANY-maze system (RRID:SCR_014289).

2.2.3 | Forced swim test

Mice were individually placed in a transparent glass cylinder (height: 70 cm; diameter: 30 cm) filled with water up to the 30 cm level, maintained at a temperature of 23 ± 1°C. Videotaping occurred over 6 min, and immobility time was calculated during the last 5 min.

2.2.4 | Tail suspension test

Each mouse was individually suspended by the tails by using adhesive tape, positioned 1 cm from the tail tip and 30 cm above the ground. The test duration was 6 min, and the immobility time was measured during the final 5 min. Video recording captured the mouse's behavior throughout the test.

2.2.5 | Three-chamber social test

The three-chamber apparatus (60×40×25 cm) consisted of three communicating chambers separated by Perspex walls, with central openings (8×12 cm) allowing access to the adjacent chambers. Two small black wire cages were positioned in the corner of the side chambers. During the first session (habituation), the mouse was initially placed in the middle chamber, with unrestricted access to the left and right chambers. Over 10 min of observation, the sniffing time (direct snout-to-enclosure contact) at both enclosures in the center of the chambers was recorded. In the second session (social ability), a different mouse (Stranger 1) was placed into one enclosure, and the experiment mouse's motions were tracked for 10 min. The time spent sniffing Stranger 1 and the empty enclosure was recorded. In the third session (social recognition), another mouse (Stranger 2) was introduced into the remaining enclosure, and the experiment mouse's motions were tracked for 10 min. The time and number of sniffing events directed at Stranger 1 and Stranger 2 were meticulously recorded.

2.2.6 | Novel object test

An open-topped box (40×40×30 cm) was placed in a dimly illuminated room. During the training session, mice were introduced to the arena and allowed to explore two identical objects for 10 min. In the subsequent test phase, conducted 90 min later, one of the two objects was replaced with a new object. The time spent exploring each object was measured over 10 min.

2.2.7 | Y-maze test

The Y-maze consisted of three arms with angles of 120°, each arm measuring 30×4.5 cm with a height of 15 cm. Unique visual cues were placed on the walls near the end of each arm. The arms were defined as the start arm, familiar arm, and novel arm. In the training session, the novel arm was closed, allowing the mouse to freely explore the other two arms (start and familiar arms) for 5 min. Subsequently, the test was conducted 90 min after the training session. The novel arm was opened, granting the mouse access to all three arms. The number of times the mouse explored the new arm and the time spent on the new arm were measured using the ANY-maze system (RRID:SCR_014289).

2.3 | Single-nucleus RNA sequencing procedures

2.3.1 | Tissue dissociation for 10× Genomics sequencing

The male pups (30 mice per group) were humanely killed through cervical dislocation under deep anesthesia induced by 3% sevoflurane suspended in air on postnatal day 37. In a swift procedure, prefrontal cortices (PFCs) were meticulously dissected from fresh mouse brain samples within an ice-cold phosphate-buffered saline solution, ensuring a consistently cold environment during the microdissection process. The dissected PFC was subsequently fragmented into smaller chunks (approximately 1–2 mm^3), placed in ice-cold RNA later (cat. no. AM7020, Ambion), and stored overnight at 4°C.

Nuclei were isolated via iodixanol (cas. no. 92339-11-2, US Pharmacopeia) gradient centrifugation, following standard procedures. A separate chunk was immersed in 500 mL lysis buffer, ground into nuclei suspension, and then combined with 700 μL resuspension buffer. The nuclei suspension was filtered through a 50-μm cell strainer (cat. no. 352350, Corning) to eliminate debris. Subsequently, 1 mL of 50% iodixanol was added to the filtrate to create a 25% nuclei/iodixanol mixture. This mixture was layered onto 33%/30% iodixanol to establish microscopic gradients for nuclei extraction. The gradient underwent centrifugation at 3234 g for 20 min at 4°C, separating nuclei from the tissue. The isolated nuclei were washed with resuspension buffer three times.

Following centrifugation at 500 g for 5 min at 4°C, the final nucleus suspension containing the desired cell fragments was obtained. This solution underwent filtration using a 40-μm strainer (cat. no. 431750, Corning) to remove debris. The nuclei were labeled with Ruby dye and subsequently counted for further analysis.

2.3.2 | Single-nucleus barcoding and library construction

Barcoded single nuclei, Gel Bead-In-Emulsions (GEMs), and cDNA libraries were generated following the established protocol from 10×Genomics Gem Code Technology (RRID:SCR_023672). Single-nucleus RNA was initially purified using Single Cell 3' Gel Bead in a GEM, wherein each transcript in the single cell was uniquely barcoded using a unique molecular identifier (UMI).

In brief, the 10x™ Gem Code™ Technology employed approximately 750000 barcodes to individually index the transcriptome of each cell. Thousands of nuclei were partitioned into GEMs, with all resulting cDNA sharing a common 10x Barcode. Subsequent incubation of the GEMs facilitated the production of barcoded, full-length cDNA from polyadenylated mRNA. Following this incubation period, the GEMs were fragmented, and the combined fractions were extracted.

Silan magnetic beads were then utilized to eliminate any residual biochemical reagents and primers from the post-GEM reaction mixture. The subsequent step involved polymerase chain reaction (PCR) amplification of the full-length, barcoded cDNA to achieve a sufficient quantity suitable for subsequent library construction.

2.3.3 | Sequencing of single-nucleus cDNA libraries

Transcripts were aligned to the Ensembl release 107 reference genome. A Single Cell 3' Library consisted of standard Illumina paired-end constructs. In Read 1, the Single Cell 3′ 16 bp 10x Barcode and 10 bp unique molecular identifier (UMI) were encoded, while Read 2 was dedicated to sequencing the cDNA fragment. Sample index sequences were included as the i7 index read. Both Read 1 and Read 2 utilized standard Illumina® sequencing primer sites in the context of paired-end sequencing (RRID:SCR_016387).

2.3.4 | Data quality control

The splicing-aware alignment of reads2 to the Ensembl release 107 reference genome was executed using STAR (Spliced Transcripts Alignment to a Reference; https://github.com/alexdobin/STAR). Subsequently, the transcript annotation GTF was utilized to categorize the reads into exonic, intronic, and intergenic regions. In the context of transcriptome reads, if reads mapped exclusively to a single gene, they were designated as uni-mapped. Only uni-mapped reads were employed in UMI counting. Following this step, Cell Ranger filtered and corrected barcodes and UMIs to derive effective cell numbers for downstream analyses.

2.3.5 | Cell clustering analysis

After removing low-grade cells from the dataset, data were normalized. A global-scaling normalization method *Log Normalize* was used to normalize the gene expression measurements for each cell by the total expression. The formula is shown as follows:

$$\text{A gene expression level} = \log(1 + (\text{UMI(A)})/(\text{UMI(TOTAL)}) \times 10000).$$

The VST method of the *Find Variable Features () function* is used to search for intercellular high-feature genes used for downstream analysis. The z-score normalization was performed on the data by *Scale Data () function* so that the mean expression of genes in each cell was equal to 0 and the variance was equal to 1. Moreover, some highly expressed genes with a dominant role in the downstream analysis were excluded. Then, the Seurat R package (https:// github.com/satijalab/Seurat), developed initially as a clustering tool, was used for these datasets onto two dimensions using t-distributed stochastic neighbor embedding (t-SNE).

2.3.6 | Identification of marker genes of individual cell clusters

Cell cluster-specific marker genes, which were expressed in at least 25% of the single cells (mincell_pct ≥0.25) and determined with *p*-value ≤0.01 and log(fold-change)(|logFC|) ≥ 0.360674 between the groups, were defined from our 10x sequencing dataset using a likelihood-ratio test (Camp et al., 2017). Then, the canonical cell-type-specific markers for major PFC cell types and neuronal subtypes from previous studies were used to resolve the identities of the cell clusters in this study.

2.3.7 | DEG and enrichment analysis

The *Find Markers* function in the Seurat was used to identify DEG analysis, after which a hurdle model in MAST (model-based analysis of single-cell transcriptomics) was used to find DEGs in each cluster, based on the following criteria: (1) |logFC| ≥ 0.36; (2) $P_{adj} \leq 0.05$; and (3) the percentage of cells ≥25%.

Gene Ontology (GO) enrichment analysis was employed to identify all significantly enriched GO terms, encompassing Cellular Component, Molecular Function, and Biological Process categories, for peak-related genes in each cell type. The analysis was based on the Gene Ontology terms available in the database (http://www.geneontology.org).

Furthermore, pathway enrichment analysis from the Kyoto Encyclopedia of Genes and Genomes (KEGG) database (https://www.genome.jp/kegg/) was conducted. This analysis aimed to identify significantly enriched metabolic pathways or signal transduction pathways in peak-related DEGs when compared with the entire genome background within each cell type.

2.3.8 | Single-cell trajectory analysis

The single-cell trajectory was reconstructed using pseudo-time analysis in Monocle 3 (Cao et al., 2019). Throughout development, cells progress through distinct "states," each characterized by unique sets of genes responsible for the synthesis of proteins and metabolites crucial for their functions. Monocle 3 utilizes an algorithm to decipher the sequence of gene expression changes occurring in each cell during a dynamic biological process. By capturing the overall "trajectory" of gene expression alterations, Monocle 3 accurately positions each cell along its corresponding point in the trajectory.

In contrast to clustering, which is compatible with both Uniform Manifold Approximation and Projection (UMAP) and t-distributed stochastic neighbor embedding (t-SNE), Monocle 3 is specifically utilized for reconstructing trajectories with multiple branches in the UMAP space. Key genes associated with the development and differentiation process along the pseudo-time course were identified, employing a false discovery rate (FDR) <0.0001 as the cutoff value. The branches in the single-cell trajectories signify distinct biological functions based on the gene expression dynamics during development.

2.4 | Selection of GWAS disease-relevant candidate genes in cell clusters

The NHGRI-EBI GWAS catalog (version 1.0.2) provided the list of GWAS candidate genes along with their associated disease. Only GWAS genes exhibiting exonic mutations were compared with differentially expressed genes (DEGs) in different cell subtypes. Subsequently, potential false-positive genes in each cell type were identified based on the following criteria: (1) genes displaying non-uniform expression across all the clusters (Shannon-entropy-based test, p-value <1e-5) and (2) genes expressed in cells concentrated within a subset of clusters, rather than being uniformly distributed across all clusters (Shannon-entropy-based test, p-value <1e-8).

After excluding the false-positive genes, the heatmap displayed enriched (1) or non-enriched (0) clusters using the kneepointDetection method. The mean expression of each cluster was calculated using cells with an expression value <99th percentile for each gene.

2.5 | Statistical analysis

A priori statistical power calculation was not conducted before the study, and the number of pup mice was determined based on insights gained from previous studies (Song, Peng, et al., 2023). No pre-determined exclusion criteria were established, except in cases where animals died during the experiment. A total of 92 mice were killed for the experiment, with 8 mice per group for behavioral tests and 30 male mice per group for single-nucleus RNA sequencing. Importantly, no mice died during the experiment.

Behavioral test data were assessed for normal distribution and homogeneity of variance using the Kolmogorov–Smirnov test and were presented as mean ± standard deviation (SD). Outlier tests were not performed. Statistical analyses were conducted using the GraphPad Prism software (version 9.0, RRID:SCR_002798). The two-tailed Student's t-test was employed to analyze the data from the open field test, elevated plus maze, forced swim test, tail suspension test, three-chamber social test, novel object test, and Y-maze test between two groups. A p-value <0.05 was considered statistically significant. For the statistical analyses and graphics production with snRNA-seq data, R (version 3.5.3, Foundation for Statistical Computing) was utilized.

3 | RESULTS

3.1 | Multiple neonatal exposures to sevoflurane-induced sexual dimorphism in sociability at the juvenile age in mice

To assess the effects of multiple neonatal exposures to sevoflurane on sociability, spatial working memory, anxiety-like behavior, and depression-like behavior, a battery of behavioral tests were performed on postnatal days (PNDs) 31–36 (Figure S1).

In the social interaction tests on PND 31, during the habituation session, both male and female mice in both groups spent a similar time sniffing the left and right empty enclosures (male control group: Left vs. Right: $t=0.914$, df = 7, $p=0.391$; male sevoflurane group: Left vs. Right: $t=0.858$, df = 7, $p=0.419$; female control group: Left vs. Right: $t=0.959$, df = 7, $p=0.370$; female sevoflurane group: Left vs. Right: $t=0.415$, df = 7, $p=0.690$; Figure 1a,d). In the sociability session, male and female mice in both groups showed normal sociability, as proven by spending more time sniffing Stranger 1 than the empty enclosure (male control group: Stranger 1 vs. Empty: $t=4.141$, df = 7, $p=0.004$; male sevoflurane group: Stranger 1 vs. Empty: $t=5.154$, df = 7, $p=0.001$; female control group: Stranger 1 vs. Empty: $t=3.658$, df = 7, $p=0.008$; female sevoflurane group: Stranger 1 vs. Empty: $t=4.998$, df = 7, $p=0.002$; Figure 1b,e). In the preference for social recognition session, male and female mice in the control group (male control group: Stranger 1 vs. Stranger 2: $t=4.943$, df = 7, $p=0.002$; female control group: Stranger 1 vs. Stranger 2: $t=5.360$, df = 7, $p=0.001$) or female mice in the sevoflurane group (female sevoflurane group: Stranger 1 vs. Stranger

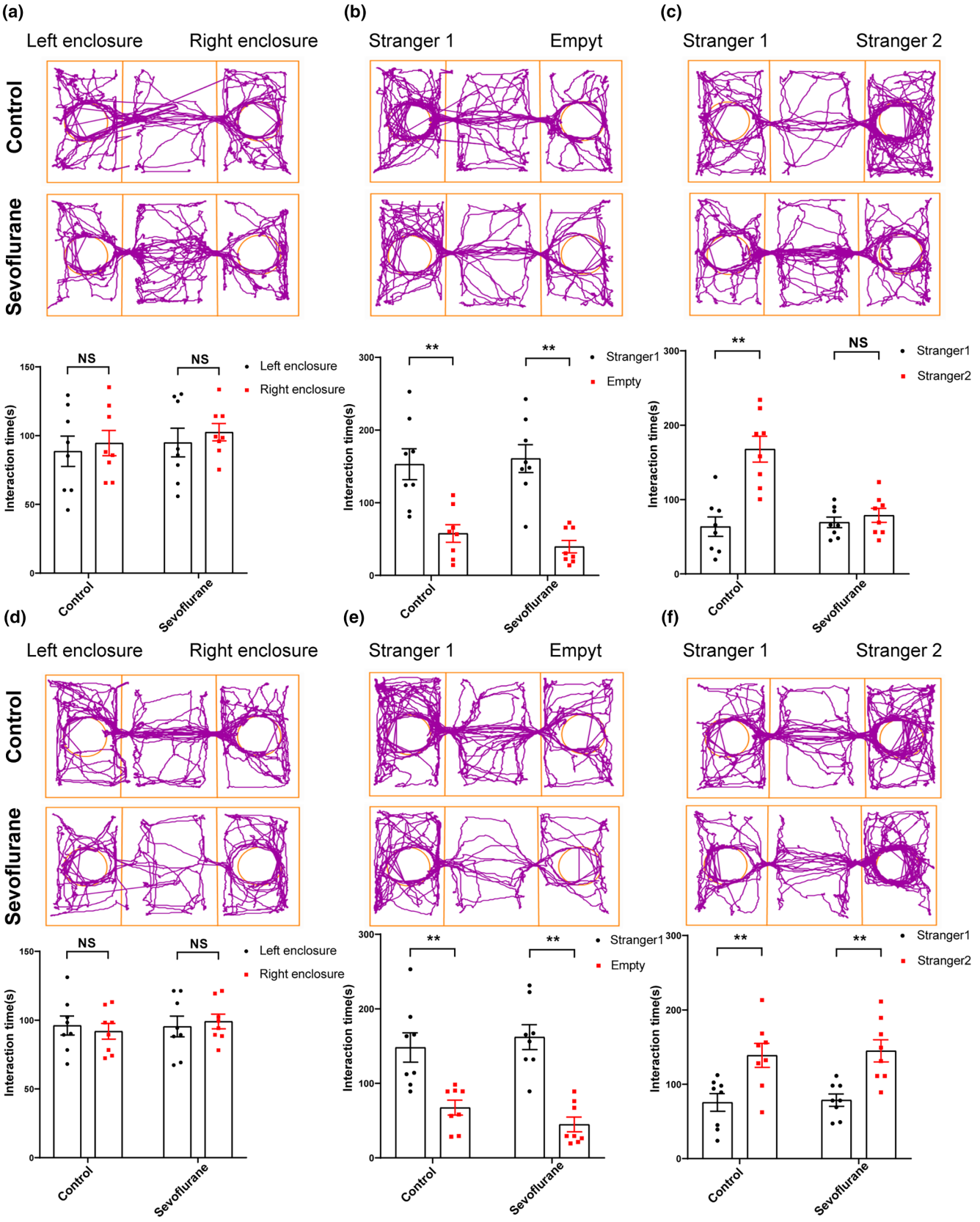

2: $t = 3.802$, df = 7, $p = 0.007$) spent more time sniffing Stranger 2 than Stranger 1, while male mice in the sevoflurane group showed no side preference (male sevoflurane group: Stranger 1 vs. Stranger 2: $t = 0.657$, df = 7, $p = 0.532$; Figure 1c,f). Together, these data suggested that multiple neonatal exposures to sevoflurane could induce sexual dimorphism-linked deficit in sociability at juvenile age.

The Y-maze test (PND 32) and novel object test (PND 33) were evaluated for spatial working memory. In the Y-maze test, mice

FIGURE 1 Multiple neonatal exposures to sevoflurane-induced sexual dimorphism in social recognition in the juvenile male mice. (a) In the sociability test on habituation, the subject male mice in either control group or sevoflurane group have no significant difference in time of sniffing at the left and right empty enclosures. (b) In the social interaction test on sociability, the male mice in both groups spent more time sniffing at Stranger 1 than at the empty enclosure. (c) In the social interaction test on social recognition, the male mice in the sevoflurane group do not prefer Stranger 2 to Stranger 1 in sniffing time. (d) In the sociability test on habituation, the subject female mice in either control group or sevoflurane group have no significant difference in time of sniffing at the left and right empty enclosures. (e) In the social interaction test on sociability, the female mice in both groups spent more time sniffing at Stranger 1 than at the empty enclosure. (f) In the social interaction test on social recognition, the female mice in both groups spent more time sniffing at Stranger 2 than Stranger 1. Data are means ± SD. $n = 8$ male mice or female mice/group. Student's *t*-test. $^{**}p < 0.01$, $^{***}p < 0.001$.

in the sevoflurane group had fewer novel arm entries (male mice: $t = 3.636$, df = 14, 81.00 ± 13.40 vs. 60.50 ± 8.65, $p = 0.003$; female mice: $t = 2.993$, df = 14, 82.88 ± 14.62 vs. 63.00 ± 11.78, $p = 0.0097$; Figure S1) and shorter time in the novel arm (male mice: $t = 3.435$, df = 14, 193.20 ± 40.48 vs. 131.00 ± 31.30, $p = 0.004$; female mice: $t = 3.706$, df = 14, 179.10 ± 29.88 vs. 121.70 ± 32.06, $p = 0.0024$; Figure S1) compared to the control group (Figure S1). In the novel object test, the sevoflurane group mice spend less time (male mice: $t = 3.162$, df = 14, 87.65 ± 27.88 vs. 50.58 ± 17.96, $p = 0.0069$; female mice: $t = 3.040$, df = 14, 85.70 ± 21.20 vs. 54.53 ± 19.80, $p = 0.0088$) and fewer numbers (male mice: $t = 3.615$, df = 14, 75.00 ± 20.16 vs. 41.00 ± 17.36, $p = 0.0028$; female mice: $t = 3.369$, df = 14, 72.75 ± 19.18 vs. 44.75 ± 13.59, $p = 0.0046$) on exploring the novel object than that in control group mice (Figure S2). The anxiety-like behavior assay showed no significant differences in the time spent in the central zone of the open arms (Figure S3). The locomotor activity in the open field test and the time spent in the central zone did not reveal any differences among the two groups (Figure S4). The forced swim test and tail suspension test detected no obvious alteration in the immobility time of sevoflurane group compared with control group (Figure S5).

3.2 | Unbiased identification of cellular populations in the PFC

Behavioral assessments indicated that repeated neonatal exposure to sevoflurane resulted in the development of sexual dimorphism in sociability during the juvenile phase. To investigate potential underlying mechanisms, single-nucleus RNA sequencing (snRNA-seq) analysis was conducted on cell nuclei (9195 nuclei in the control group and 7082 nuclei in the sevoflurane group were detected) extracted from specific sections of the PFC, including the anterior cingulate, prelimbic, and infralimbic cortex. The analysis included both male control mice ($n = 30$) and those exposed to sevoflurane ($n = 30$; Figure 2a).

After rigorous data pre-processing and quality control procedures, 8489 high-quality cell nuclei were identified in the PFC of control male mice (with a median of 37 832 UMIs and 1227 genes/cell), while 6619 cell nuclei were obtained from sevoflurane-exposed male mice (with a median of 58 661 UMIs and 1393 genes/cell; Figure S6). The raw sequence data have been archived in the Sequence Read Archive (SRA) submission: SUB13480335 of the National Center for Biotechnology Information (NCBI) under accession No. PRJNA979330 (SUB13480335—Summary | Sequence Read Archive (SRA) | Submission Portal (nih.gov)). To effectively categorize these cells, modularity optimization techniques (SLM algorithm: smart local moving algorithm) and t-SNE were employed, revealing 8 distinct major cell clusters with similar transcriptomic profiles (Figure 2b).

Based on established cell-type-specific markers (Zeisel et al., 2015), eight distinct cell populations within the PFC were successfully identified across all samples. These populations included astrocytes expressing Apoe$^+$ in four subtypes (Cst3$^+$, Ptgds$^+$, Slc38a2$^+$, and VTN$^+$), microglia expressing C1qa in two subtypes (Ctss$^+$ and Apoe$^+$), oligodendrocytes marked by Mbp, OPCs identified through Pdgfra, endothelial cells characterized by Flt1, hypothalamic ependymal cells denoted by Tmem212, choroid plexus epithelium designated by krt18, and neurons expressing Snap25, further classified as glutamatergic (Slc17a7$^+$), GABAergic (Gad2$^+$), and Dcc$^+$ neurons (Figure 2b,c).

Additionally, novel marker genes specific to each cell type within the PFC were uncovered, including *hs3st4* for glutamatergic neurons, *Dlx6os1* for GABAergic neurons, *slc7a11* for astrocytes, *Runx1* for microglia, and *C030029H02Rik* for oligodendrocytes (Figure 2d). Notably, the preponderance of glutamatergic neurons (50.6% in control group, 48.2% in sevoflurane group) compared to the smaller proportion of GABAergic neurons (7.0% in control group, 6.5% in sevoflurane group) within the PFC mirrors the conventional excitatory/inhibitory ratio seen in cortical regions (Bhattacherjee et al., 2019; Figure 2e and Table S1).

3.3 | Expression of cell-type-specific DEGs in developmental sevoflurane neurotoxicity in the PFC

In a dual-pronged analysis, we aimed to understand cell-type-specific alterations in gene expression within the PFC following multiple neonatal exposures to sevoflurane. First, the model-based analysis of single-cell transcriptomics (MAST) identified 355 significantly up-regulated genes and 492 significantly down-regulated genes across all cell types ($P_{adj} < 0.05$, $|\log FC| \geq 0.36$), as shown in Figure 3a and Table S2. Subsequently, we investigated the impact of sevoflurane-induced neurotoxicity on gene expression in each major cell type. Notably, glutamatergic neurons (1208 DEGs), oligodendrocytes (873 DEGs), and astrocytes (188 DEGs) exhibited the most

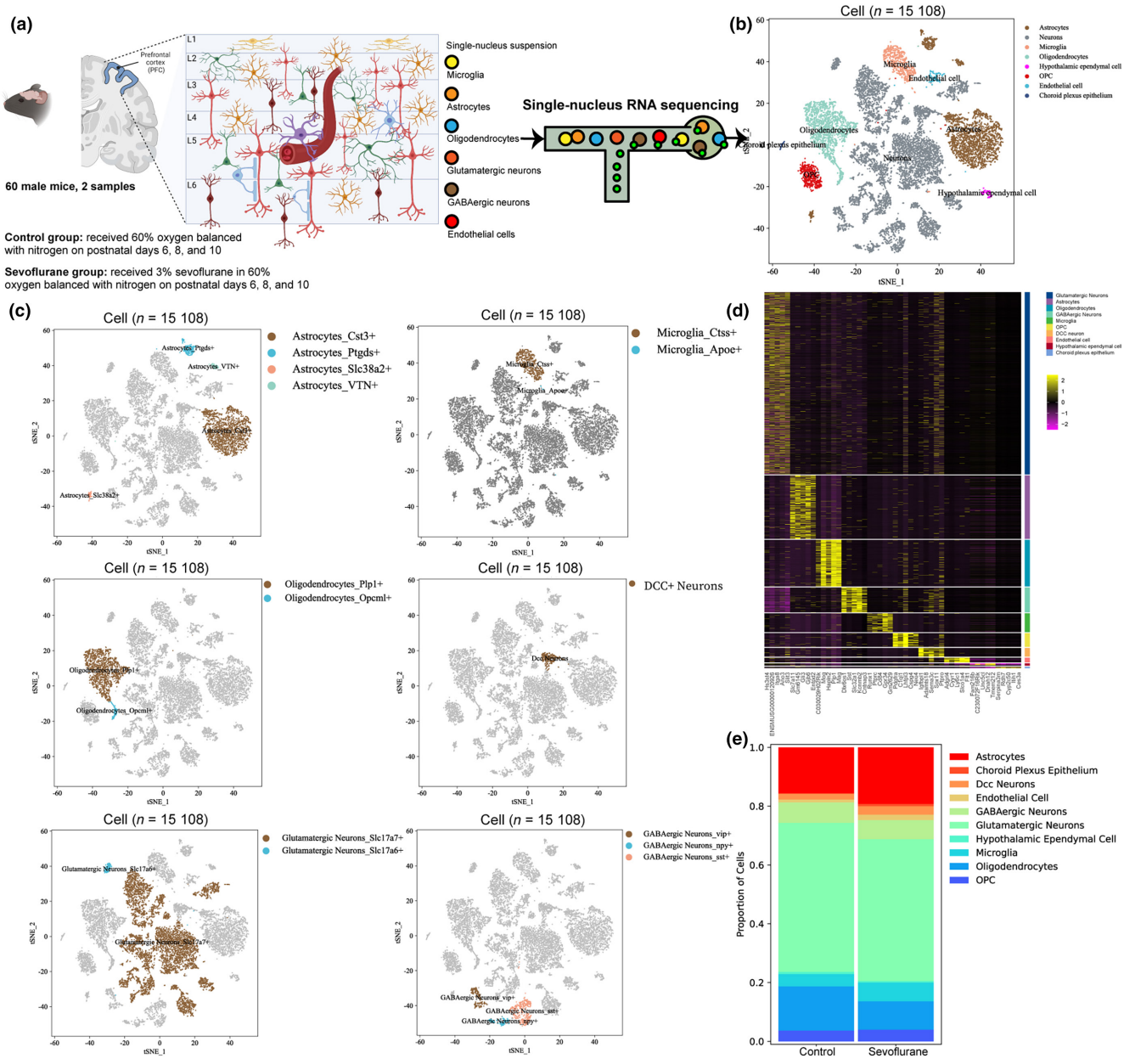

FIGURE 2 Single-nucleus RNA sequencing (snRNA-seq) analysis of the prefrontal cortex (PFC) in male mice. (a) Experimental workflow of snRNA-seq of male mice PFC from dissection through analysis. (b) The t-distributed stochastic neighbor embedding (t-SNE) plot of all 15 108 nuclei used for analysis. Clustering analysis revealed 8 broad categories of cell-type identity based on transcriptome. (c) t-SNE plots of all known cell markers in PFC clusters. *Apoe* for astrocytes with 4 subtypes (*Cst3*$^+$, *Ptgds*$^+$, *Slc38a2*$^+$, and *VTN*$^+$), *C1qa* for microglia with 2 subtypes (*Ctss*$^+$ and *Apoe*$^+$), *Mbp* for oligodendrocytes with 2 subtypes (*Plp1*$^+$ and *Opcml*$^+$), and *Snap25* for neurons divided into glutamatergic (*Slc17a7*$^+$), GABAergic (*Gad2*$^+$), and *Dcc*$^+$ neurons. (d) Single-cell heatmap highlighting cell-type-specific gene marker expression in each cluster. (e) Color-coded histogram showing the percentage of cells in each cluster in both groups.

substantial numbers of DEGs in response to neonatal sevoflurane exposures (Figure 3b). Additionally, the coefficient of variation (c.v.) within these major cell types showed a discernible downward trend after repeated sevoflurane exposures (Figure 3c), suggesting a potential reduction in the variability of gene expression post-multiple neonatal sevoflurane exposures across most cell types, which could contribute to the onset of neurotoxicity-induced cellular dysfunction within the PFC (Battle et al., 2017; Mar et al., 2011).

Subsequently, gene set enrichment analysis (GSEA) was performed to further investigate the impact of DEGs on cellular processes influenced by sevoflurane-induced neurotoxicity across diverse cell types within the PFC, utilizing the top hallmark gene set (Figure 3d and Data S3). Microglia displayed an up-enrichment (positively normalized enrichment score) of DEGs linked to the fatty acid metabolism pathway, potentially indicating microglial activation and ensuing inflammation (Chen et al., 2022). In Dcc$^+$ neurons,

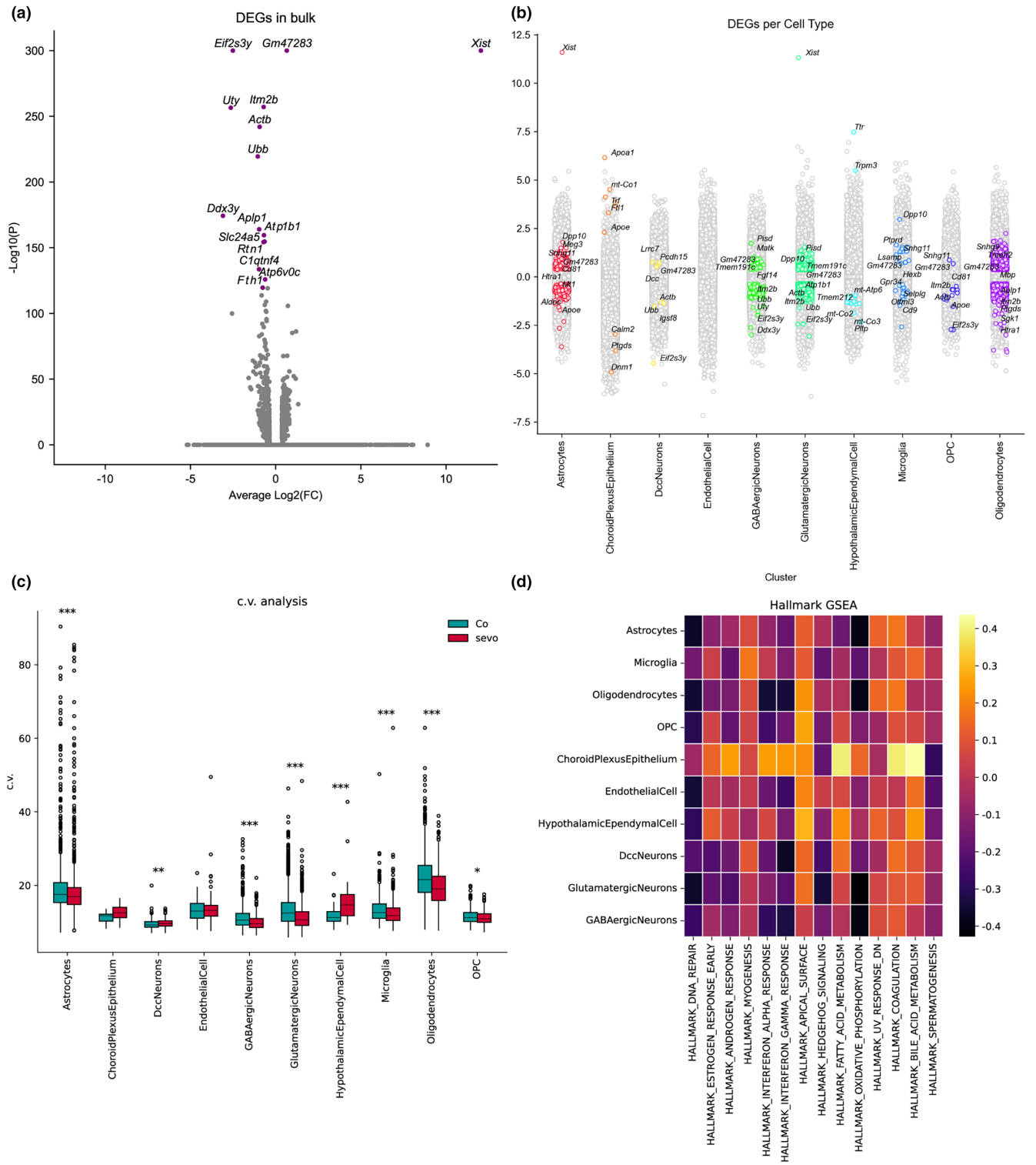

FIGURE 3 Differentially expressed genes (DEGs) and cell-type-specific translational changes in the PFC. (a) Volcano plot showing expression of DEGs between control group and sevoflurane group (P_{adj} <0.05, FC >0.36, MAST analysis with Bonferroni adjustment of *p* values). (b) Strip plot showing DEGs in each cell type with significant genes in color (P_{adj} <0.05, FC >0.36, MAST analysis with Bonferroni's adjustment of *p* values). Top five up-regulated and down-regulated genes per cluster labeled. (c) Coefficient of variation (c.v.) analysis for each cell type. In almost all subtypes, the c.v. is significantly lower in the sevoflurane group (two-sided Wilcoxon's test with Bonferroni's correction, $^{*}P_{adj}$ =0.05, $^{**}P_{adj}$ =0.01, $^{***}P_{adj}$ <0.001, n =24 876 genes in the control group and n =24 975 genes in the sevoflurane group; n =30 mice/group). Box indicates range from 25th to 75th percentiles, with whiskers extending to 1.5 times the interquartile range. (d) Heatmap showing GSEA for hallmark terms. Color indicates normalized enrichment score (NES). Significant gene sets are calculated as P_{adj} <0.1.

up-regulated DEGs were prominently enriched in processes associated with thiamine metabolism. Shared molecular signatures among certain cell types were observed in the GSEA after repeated neonatal sevoflurane exposures. For instance, glutamatergic neurons, GABAergic neurons, oligodendrocytes, and astrocytes collectively exhibited the down-regulated enrichment of DEGs in the oxidative phosphorylation signaling gene set, the primary pathway for neuron energy production (Sobieski et al., 2017). This highlights the weakness of the oxidative phosphorylation pathway within the PFC and provides fresh insights into the developmental neurotoxicity triggered by sevoflurane exposure.

Conventional bulk tissue genetic sequencing analysis tends to obscure cell-type-specific transcriptomic profiles, particularly within less prevalent cell populations such as neuron subclusters. To address this limitation, we focused on identifying cell-type-specific DEGs within each distinct cell cluster, unraveling crucial GO enrichments (Data S4) and signaling pathways (Data S5). Notable findings include 1682 DEGs within glutamatergic neurons, 47 DEGs within GABAergic neurons, and 168 DEGs within astrocytes (Figure S7 and Data S6). These distinct DEGs, specific to each cell type and differentially expressed between the control and sevoflurane-exposed groups, can potentially unveil intricate mechanisms underpinning sevoflurane-induced neurotoxicity, offering nuanced insights that conventional bulk tissue studies may overlook.

3.4 | Neuronal subtype distinct layers in the PFC

Cortical glutamatergic neurons exhibit distinct laminar organization closely tied to their relays, interconnections, and functions (Shipp, 2007). General anesthetics have been shown to modulate layer-specific cortical activity and selectively alter the states of pyramidal neurons in specific layers (Bharioke et al., 2022). However, few studies have delved into the impact of multiple neonatal sevoflurane exposures on each layer of the prefrontal cortex (PFC). In this study, we identified 15 transcriptionally distinct glutamatergic neuron subclusters (Figure 4a) with unique markers (Figure 4b). t-SNE plots illustrated the landscape of each unique marker in respective neuron populations (Figure S8). Given that the PFC comprises five layers (L1, L2, L3, L5, and L6), we re-identified 16 glutamatergic neuron subclusters across all samples within the PFC based on known layer marker genes (Bhattacherjee et al., 2019). Subcluster 10, enriched with *Reln*$^+$, belonged to the L1; subcluster 12 with *Tshz2*$^+$ was located in the L2; subclusters 2, 3, 5, 11, and 13 were part of L2/3 defined by *Cux2*$^+$; subcluster 0 was also a part of L2/3 defined by *Calb1*$^+$; subclusters 1 and 7 with *Etv1*$^+$ and cluster 15 with *Pop4*$^+$ were in L5; subcluster 4, 8, and 9 with *Cpne4*$^+$ were enriched within L5/6; and subcluster 6 with *Foxp2*$^+$ enrichment was positioned in L6 (Figure 4c; Figure S9). Quite unexpectedly, subcluster 14, which included a very small subset of cells, had the character of microglia functions, because of its highly expressed marker genes such as *Csf1r*$^+$, *C1qa*$^+$, *Ctss*$^+$, and *C1qb*$^+$.

We subsequently verified the visualized localization of the novel cell markers (Figure 2b) in each subcluster based on the Allen Brain Atlas in situ hybridization (ISH) images (Figure 4d; Figure S10). However, subcluster 1 marker gene *Fibcd1* in our results was enriched in the L2/3 using Allen Brain Institute in situ hybridization, which proved *Fibcd1* was L2/3 marker gene and subcluster 1 belonged to Layer2/3. So, all the identified glutamatergic neuron subcluster markers underwent further immunofluorescence probe localization. Moreover, glutamatergic neuron subcluster markers in our findings might be more accurate than previously reported markers. To discern the functional changes in each layer of the PFC underlying developmental sevoflurane neurotoxicity, we identified DEGs enriched in distinct layers and explored the corresponding GO and KEGG pathways between the control and sevoflurane groups. This analysis aimed to elucidate the layer-specific function of glutamatergic neurons in developmental sevoflurane neurotoxicity within the PFC (Data S7). Consequently, we re-defined glutamatergic neurons based on their layer identity to provide additional evidence for specific transcriptional programs associated with developmental sevoflurane neurotoxicity in the PFC. Given the diversity of layers exhibiting apparent transcriptional changes after sevoflurane treatment, future experimental validation will be essential for a thorough analysis of layer-specific degeneration.

Previous studies have demonstrated that the GABAergic neurons did not possess distinct laminar organization, although some subpopulations may be specially located within particular layers. Canonical markers were used to identify three distinct GABAergic subclusters such as *Sst*$^+$, *Vip*$^+$, and *Npy*$^+$ GABAergic neurons (Figure 4e). Meanwhile, we partitioned these GABAergic neurons into 7 subclusters in the higher resolution (Figure 4f) and summarized transcriptional changes in the PFC using the KEGG gene sets and Go analysis after multiple neonatal sevoflurane exposures. With the results of our study, the *Vip*$^+$ GABAergic neurons can be further classified into three broad subtypes based on the expression of *Adarb2*$^+$, *Cacna2d1*$^+$, and *Zfpm2*$^+$. Importantly, we detected at least four distinct GABAergic neuron subpopulations that do not belong to any of the principle *Sst*$^+$, *Vip*$^+$, and *Npy*$^+$ populations, such as subtype 0 (*Slit2*$^+$) and subtype 6 (*Kit*$^+$). Besides excitatory and inhibitory neurons, we also detected *Dcc*$^+$ neurons in the PFC, which had no layer properties. In summary, we discovered some novel neuron subtypes without layer identity and provided a new perspective on the functions of individual nerve cell types underlying sevoflurane neurotoxicity in the PFC.

3.5 | Trajectory analysis from OPCs to oligodendrocytes in the PFC

Oligodendrocyte progenitor cells (OPCs) continually generate myelin-forming cells (oligodendrocytes, OLs) to maintain myelination in the central nervous system throughout life (Azim et al., 2017). Recent pre-clinical studies have indicated that multiple exposures to

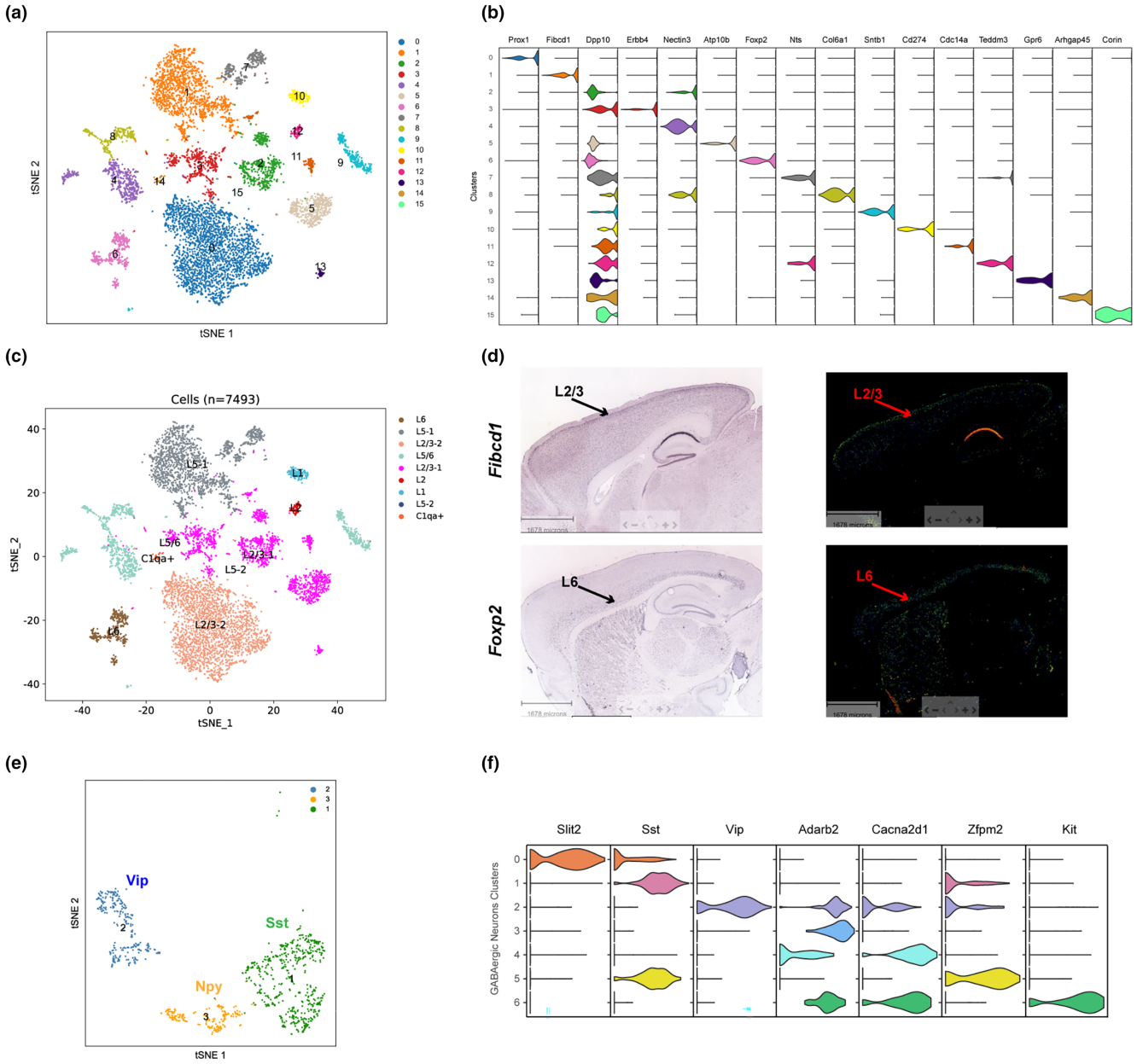

FIGURE 4 Distinct layers of neuronal subtypes in the PFC. (a) t-SNE plot showing that glutamatergic neurons are broadly classified into 16 subclusters in the PFC. (b) Violin plot showing expression of specific markers for each of the 16 glutamatergic neuron subclusters. (c) t-SNE plot showing that glutamatergic neuron subclusters are allocated into specific cortical layers by projecting expression of layer-specific markers. (d) The unique markers in distinct glutamatergic neuron subclusters identified by our single-cell sequencing approach were validated using the in situ hybridization images in the Allen Brain Atlas (https://mouse.brain-map.org). (e) t-SNE plot showing identification of PFC GABAergic neurons into 3 distinct subtypes based on canonical markers. (f) Violin plot showing expression of specific markers of GABAergic neurons which can be furtherly classified into 7 subclusters based on their transcriptome in the PFC. $n = 30$ mice/group.

anesthesia could inhibit OL myelination in the developing nervous system, with the PFC being more susceptible to demyelination (Liang et al., 2021). However, a detailed description of the differentiation from OPCs to OLs in the PFC after multiple sevoflurane exposures is lacking, obscuring the understanding of sevoflurane neurotoxicity. To address this, we illustrated the trajectory from OPCs to OLs through the pseudo-temporal ordering of nuclei in the PFC between the control group and the sevoflurane group (Figure 5a). We visualized the differential expression of top genes across pseudo-time in both groups, determining flexible differentiation branches (Figure 5b; Table S8).

Our results revealed that the endpoint of OL differentiation typically halted in nodes N.O. 1–6 under normal circumstances. However, pseudo-time trajectory analysis demonstrated that multiple sevoflurane exposures led to nodes getting stuck in N.O. 7–13 (Figure 5c). A distinct separation between cells from sevoflurane-treated mice and controls was observed in both OPCs and oligodendrocytes. To explore how the key genes regulate

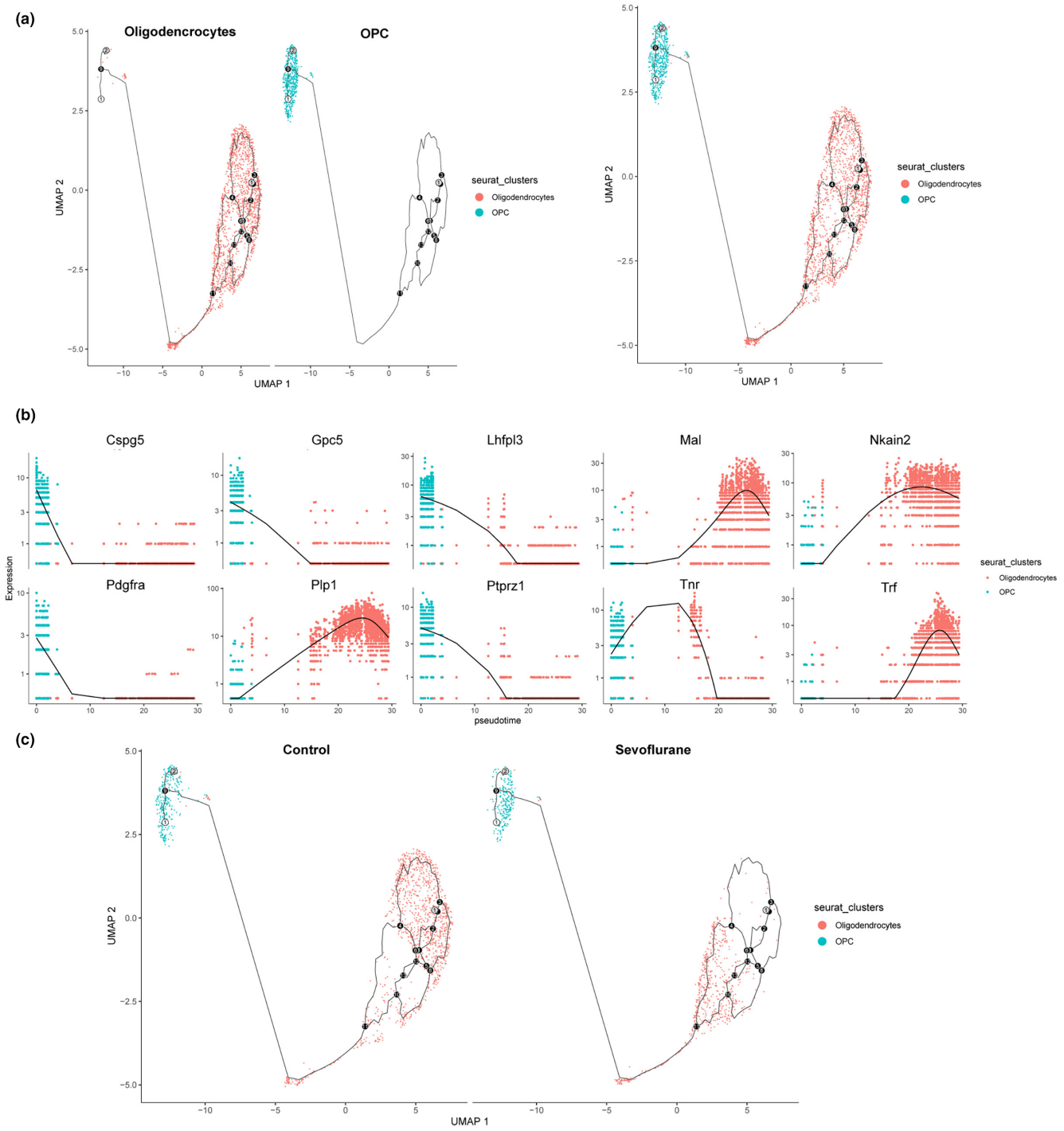

FIGURE 5 Changes in differentiation trajectory from oligodendrocyte precursor cells (OPCs) to oligodendrocytes (OLs) induced by sevoflurane exposures in the PFC. (a) Differentiation trajectory of OPCs and OLs (left) and merge trajectory from OPCs to OLs (right) in two dimensions in both groups. (b) Differential expression of top 10 genes across pseudo-time in both groups. Criteria for top genes: false discovery rate less than 1e-5 (Monocle 2 package). $n = 1710$ cells (control group) and $n = 963$ cells (sevoflurane group). (c) Differentiation trajectory from OPCs to OLs in the control group (left) and sevoflurane group (right) in two dimensions. $n = 30$ mice/group.

differentiation branch nodes in the PFC, we visualized DEGs between N.O. 1-6 branch nodes (control group) and N.O. 7-13 branch nodes (sevoflurane group) across pseudo-time, overlapping with bulk genes (Figure S11). We identified 598 key genes that may contribute to the sevoflurane-induced interruption of the differentiation trajectory between OPCs and OLs after multiple neonatal sevoflurane exposures in the developing PFC in mice. Subsequently, we annotated these key genes with enriched GO and KEGG pathways to elucidate their crucial role in neurotoxicity within this trajectory (Figure S12; Table S9). Further experimental validation will focus on the nervous system class (long-term potentiation, synaptic vesicle cycle, and retrograde endocannabinoid

signaling) and signal transduction class (MAPK signaling pathway, ErbB signaling pathway, and Ras signaling pathway), which may be relevant to the aberrant myelination.

3.6 | Identification of neurobehavioral disease risk genes in the PFC

The PFC has been implicated in various neuropsychiatric disorders, including social dysfunction, working memory impairment, autism, schizophrenia, bipolar disorder, psychosis, mania, depression, and suicidal tendencies (Paus et al., 2008). Our behavior results, along with previous studies, have confirmed that multiple neonatal exposures to sevoflurane can induce impairment in working memory (Song et al., 2019). Furthermore, our findings suggest that repeated sevoflurane exposures can lead to sexual dimorphism in social dysfunction during the juvenile age in mice. The transcriptional plasticity induced by sevoflurane exposure is believed to play a key role in the pathogenesis of these disorders.

To identify risk genes with cell-type-specific expression in the PFC that are associated with neurobehavioral disorders, we conducted a genome-wide association study (GWAS) using candidate genes obtained from the EMBL GWAS catalog (https://www.ebi.ac.uk/gwas/). Our analysis revealed several neurobehavioral disease-relevant genes that were highly enriched in specific cell types of the PFC. The heatmap in Figure 6a illustrates the expression of candidate genes associated with working memory impairment, while Figure 6b depicts the number of candidate genes impacting each subtype on the global PFC t-SNE. Specifically, the social impairment candidate gene (*Lhfpl3*) was found to be enriched in specific cell types of the PFC (Figure 6c,d). Additionally, we identified cell-type-specific GWAS candidate genes associated with other PFC-related disorders, such as autism and attention-deficit/hyperactivity disorder (ADHD; Figure 6e; Figure S13; Table S10). These cell-type-specific GWAS candidate genes provide valuable insights into the mechanisms underlying neurobehavioral disorders induced by multiple neonatal sevoflurane exposures.

4 | DISCUSSION

In this snRNA-seq study, we meticulously analyzed a total of 15 108 nuclei, with 8489 derived from the control group and 6619 from the sevoflurane-exposed group, providing a comprehensive cellular atlas of the PFC in male mice. Our investigation revealed eight distinct cell populations, each characterized by unique transcriptional features. The observed findings suggest extensive transcriptional adaptations within each cell type during the juvenile age in male mice following multiple neonatal exposures to sevoflurane.

Consistent with our results, previous studies have reported that multiple sevoflurane exposures can lead to working memory impairment in both male and female mice (Kodama et al., 2011; Xu et al., 2018). Moreover, our behavioral assessments demonstrated that sevoflurane exposures induced sexual dimorphism in sociability deficits, with significant effects observed in males but no discernible changes in females. Importantly, these neurobehavioral disorders are intricately linked to the functions of the PFC. Subsequently, we conducted snRNA-seq analysis of the PFC at postnatal day 37 to delve into the molecular mechanisms underlying these effects in male mice. Through this approach, we successfully delineated eight broad cellular subtypes, encompassing glutamatergic neurons, GABAergic neurons, various non-neuronal populations, and PFC-specific cell types such as DCC^+ neurons. Our data show that multiple neonatal exposures to sevoflurane affect transcriptome profiling across neuronal and non-neuronal cells and do not alter cell-type proportions except oligodendrocytes. The snRNA-seq strip plot highlighted a large number of special cell-type genes highly responsive to sevoflurane in the PFC, including several down-regulated gene expressions (*Itm2b* in the glutamatergic neurons, *Eif2s3y* in the GABAergic neurons, *Apoe* in the astrocytes, and *Ptgds* in the oligodendrocytes) and up-regulated expression of *Snhg11* in the microglia, which may represent potential molecular targets for sevoflurane neurotoxicity (Figure 3b). Interestingly, *Xist* was over-expressed in almost all cell types, which may lead to sevoflurane-induced social and emotional impairment (Xu et al., 2021).

Notably, the PFC displays some degrees of histological laminar organization (Shipp, 2007). The t-distributed stochastic neighbor embedding plots showed 15 glutamatergic neuron subclusters in the PFC of male mice (Figure 4a). To explore the influence of repeated sevoflurane exposures on different layers in the PFC, we divided these subclusters into 5 groups (L1, L2, L3, L5, and L6). The DEGs (Data S7) between control and sevoflurane groups were enriched in neurodegenerative disease pathways related to Parkinson's disease, Huntington's disease, and prion disease in the L2/3–1, L2/3–2, L5, and L5/6. However, the annotation of the DEGs in the L6 was enriched in the axon guidance and oxytocin signaling pathways, which may be a remarkable step forward in molecular-based therapy for social dysfunction.

Compared with glutamatergic neuron subclusters, the GABAergic neurons in the PFC showed less abundance in cellular heterogeneity. Our results showed that GABAergic neurons could be classified into 3 subclusters (Sst^+, Vip^+, and Npy^+), which could be further separated into 6 subclusters at a higher resolution. We also identified novel or combinatorial markers for these 6 GABAergic neuron subtypes, such as *Slit2* for subcluster 0. The aspects of changes in these newly defined subclusters may provide new insights into sevoflurane-induced developmental neurotoxicity. Importantly, we identified a new kind of neuron, the Dcc^+ neurons. Compared with the control group, *Dcc* gene was highly over-expressed in the Dcc^+ neurons in the sevoflurane group, which was linked to cognitive impairment, neurobehavioral deficit, depression-like behavior, and high susceptibility to drugs of abuse (Morgunova et al., 2020). Therefore, these findings suggested that *Dcc* up-regulation is an essential feature of sevoflurane-induced neurotoxicity in the PFC.

Recent research has highlighted the toxic effects of neonatal repeated sevoflurane exposure on myelinization (Liang et al., 2021). In

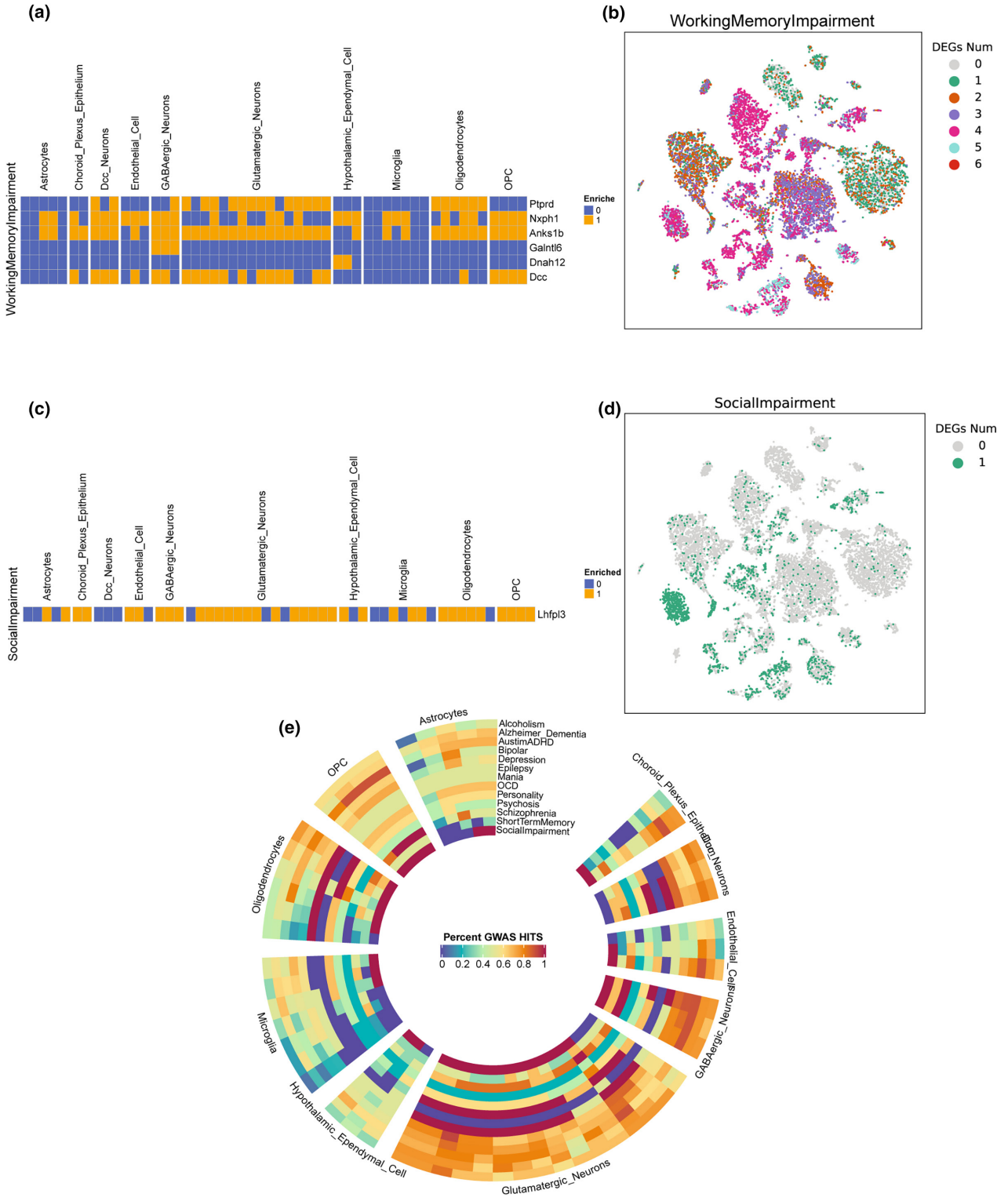

FIGURE 6 Expression of many GWAS candidate disease-relevant genes in the working memory impairment and social dysfunction is enriched in specific clusters in the PFC after multiple neonatal sevoflurane exposures. (a) Heatmap showing GWAS candidate genes with cell-type-specific expression in the working memory impairment. The blue color indicates no enrichment, and the orange color indicates gene enrichment. (b) t-SNE plot indicating the number of differentially expressed GWAS candidates in each cluster in the working memory impairment between control group and sevoflurane group. (c) Heatmap showing GWAS candidate genes with cell-type-specific expression in the social dysfunction. The blue color indicates no enrichment, and the orange color indicates gene enrichment. (d) t-SNE plot indicating the number of differentially expressed GWAS candidates in each cluster in the social dysfunction between control group and sevoflurane group. (e) Circular heatmap showing the percent of enriched subtype- and cell-type-specific GWAS candidate genes in each of the 13 PFC-relevant diseases. Bright red: high enrichment; dark blue: low enrichment.

this study, we sought to unravel the impact of multiple sevoflurane exposures on the differentiation trajectory from OPCs to OLs in the PFC. The N.O. 1 branch node represents the endpoint of differentiation during the pseudo-temporal trajectory in the OLs. In the control group, the branch nodes predominantly gathered in the N.O. 1-6, indicating a more accessible path to the myelination. Conversely, multiple sevoflurane exposures had a detrimental effect on myelination in the sevoflurane-exposed group, as evidenced by the branch nodes being stuck in the N.O. 7-13, significantly distant from N.O. 1 in the two-dimensional diagram. A comparative analysis between N.O. 1-6 and N.O. 7-13 branch nodes revealed that the Wnt signaling pathway, Ras signaling pathway, MAPK signaling pathway, and ErBb signaling pathway might play a disruptive role in the differentiation from OPCs to OLs (Figure S12). Moreover, several genes emerged as strong indicators of myelination. These findings shed light on the potential molecular mechanisms underlying the interference with myelination processes following multiple neonatal sevoflurane exposures in the developing PFC. For example, *Plp1* and *Trf* could promote differentiation from OPCs to OLs (Figure 5b); however, their expression is dynamically down-regulated in the sevoflurane group, while *Lhfpl3* representative of the resting state in the differentiation trajectory was highly expressed in the sevoflurane group. The substantial transcriptional effect and in-depth investigation of the transcriptional change will be performed in further studies. Notably, our result cannot be the first evidence of sevoflurane-induced damage to oligodendrocyte maturation.

To explore the underlying relationship between gene function and psychiatric disorders, we compared each disease-relevant GWAS mutation in humans with cell-type-specific expression pattern of DEGs in male mice. In the working memory impairment disorder, *Anks1b* (Nudel et al., 2022) was regulated in all glutamatergic neuron subclusters, GABAergic neuron subclusters, OPC subclusters, and OL subclusters. Only *Lhfpl3* was detected in GWAS mutation about the social impairment, which needs further functional verification. Furthermore, autism and attention-deficit/hyperactivity disorder (ADHD) share common behavioral phenotypes, including social difficulties, inattention, and differences in learning style, which were also validated in this model (Sokolova et al., 2017). Our findings detected 10 genes in GWAS for autism and ADHD; for example, *plcl1* (Zheng et al., 2021), *Ank3* (Leussis et al., 2013), or *syne1* (Gassó et al., 2016) was widely associated with measures of working memory and social behavior. Collectively, these psychiatric disorders strongly influenced glutamatergic or GABAergic neurons, as well as non-neuronal cells, which could cause disruptions of major support systems such as myelination.

The present study is not without its limitations. Firstly, the analysis of single-nucleus RNA sequencing (snRNA-seq) was conducted exclusively on prefrontal cortex (PFC) cells from male mice, as social interaction disorder was observed in this group. To comprehensively understand the sevoflurane-induced sexual dimorphism in sociability during the juvenile age in mice, further comparisons between male and female mice are warranted. Secondly, our investigation was restricted to a single time point (postnatal day 37) for exploring potential long-term effects through snRNA-seq. To gain a more comprehensive understanding of when and how transcriptional changes occur after multiple neonatal sevoflurane exposures, an examination of the acute phase is essential. Lastly, the limited number of animals per analysis necessitates future experiments to validate our results and confirm the identified cell clusters.

5 | CONCLUSIONS

Our study reveals the major cell-type atlas and the transcriptional profiles in the PFC of the male mice after multiple neonatal sevoflurane exposures. Our findings encompass cell-type-specific DEGs, the trajectory of differentiation from oligodendrocyte progenitor cells (OPCs) to oligodendrocytes (OLs), and the identification of psychiatric disease-relevant candidate genes across major cell types. The outcomes of this snRNA-seq investigation provide a comprehensive database, offering an advanced mechanistic understanding and facilitating the development of highly targeted therapeutic strategies for addressing developmental sevoflurane neurotoxicity.

AUTHOR CONTRIBUTIONS

Bao-jian Zhao: Writing – original draft; project administration; formal analysis; data curation. **Shao-yong Song:** Writing – original draft; formal analysis; software. **Wei-ming Zhao:** Project administration; data curation. **Han-bing Xu:** Data curation; software; formal analysis; validation. **Ke Peng:** Data curation; writing – review and editing. **Xi-sheng Shan:** Formal analysis; software; methodology; supervision. **Qing-cai Chen:** Methodology; formal analysis; data curation. **Hong Liu:** Conceptualization; methodology; writing – review and editing. **Hua-yue Liu:** Conceptualization; writing – review and editing; methodology. **Fu-hai Ji:** Conceptualization; methodology; funding acquisition; writing – review and editing; supervision.

ACKNOWLEDGMENTS

This work was supported by the National Natural Science Foundation of China (82001126, 82072130), Key Medical Research Projects in Jiangsu Province (ZD2022021), Six Talent Peaks Project in Jiangsu Province (WSN-022), Suzhou Clinical Medical Center for Anaesthesiology (Szlcyxzxj202102), Jiangsu Medical Association Anaesthesia Research Project (SYH-32021-0036 (2021031)), Suzhou Medical Health Science and Technology Innovation Project (SKY2022136), and Gusu Health Talent Project of Soochow (GSWS2021062). We thank Suzhou Dynamic Biosystems Co., Ltd for assisting in sequencing and Guangzhou Genedenovo Biotechnology Co., Ltd for bioinformatics analysis.

All experiments were conducted in compliance with the ARRIVE guidelines.

CONFLICT OF INTEREST STATEMENT

The authors declare no competing interests.

PEER REVIEW

The peer review history for this article is available at https://www.webofscience.com/api/gateway/wos/peer-review/10.1111/jnc.16068.

DATA AVAILABILITY STATEMENT

Primary data can be obtained from the corresponding author upon reasonable request. The raw sequence data have been archived in the Sequence Read Archive (SRA) submission: SUB13480335 of the National Center for Biotechnology Information (NCBI) under accession No. PRJNA979330 (SUB13480335—Summary | Sequence Read Archive (SRA) | Submission Portal (nih.gov)).

ORCID

Shao-Yong Song https://orcid.org/0000-0003-3952-2503
Wei-Ming Zhao https://orcid.org/0000-0001-6238-1679
Han-Bing Xu https://orcid.org/0009-0006-9214-0490
Ke Peng https://orcid.org/0000-0003-2879-1759
Xi-Sheng Shan https://orcid.org/0000-0003-4779-1906
Hong Liu https://orcid.org/0000-0003-3611-7131
Hua-Yue Liu https://orcid.org/0000-0002-1504-1310
Fu-Hai Ji https://orcid.org/0000-0001-6649-665X

REFERENCES

Azim, K., Angonin, D., Marcy, G., Pieropan, F., Rivera, A., Donega, V., Cantù, C., Williams, G., Berninger, B., Butt, A. M., & Raineteau, O. (2017). Pharmacogenomic identification of small molecules for lineage specific manipulation of subventricular zone germinal activity. *PLoS Biology*, *15*, e2000698.

Battle, A., Brown, C. D., Engelhardt, B. E., & Montgomery, S. B. (2017). Genetic effects on gene expression across human tissues. *Nature*, *550*, 204–213.

Bharioke, A., Munz, M., Brignall, A., Kosche, G., Eizinger, M. F., Ledergerber, N., Hillier, D., Gross-Scherf, B., Conzelmann, K. K., Macé, E., & Roska, B. (2022). General anesthesia globally synchronizes activity selectively in layer 5 cortical pyramidal neurons. *Neuron*, *110*, 2024–2040. e10.

Bhattacherjee, A., Djekidel, M. N., Chen, R., Chen, W., Tuesta, L. M., & Zhang, Y. (2019). Cell type-specific transcriptional programs in mouse prefrontal cortex during adolescence and addiction. *Nature Communications*, *10*, 4169.

Camp, J. G., Sekine, K., Gerber, T., Loeffler-Wirth, H., Binder, H., Gac, M., Kanton, S., Kageyama, J., Damm, G., Seehofer, D., Belicova, L., Bickle, M., Barsacchi, R., Okuda, R., Yoshizawa, E., Kimura, M., Ayabe, H., Taniguchi, H., Takebe, T., & Treutlein, B. (2017). Multilineage communication regulates human liver bud development from pluripotency. *Nature*, *546*, 533–538.

Cao, J., Spielmann, M., Qiu, X., Huang, X., Ibrahim, D. M., Hill, A. J., Zhang, F., Mundlos, S., Christiansen, L., Steemers, F. J., Trapnell, C., & Shendure, J. (2019). The single-cell transcriptional landscape of mammalian organogenesis. *Nature*, *566*, 496–502.

Chen, C., Liao, J., Xia, Y., Liu, X., Jones, R., Haran, J., McCormick, B., Sampson, T. R., Alam, A., & Ye, K. (2022). Gut microbiota regulate Alzheimer's disease pathologies and cognitive disorders via PUFA-associated neuroinflammation. *Gut*, *71*, 2233–2252.

Cheng, Y., Liu, S., Zhang, L., & Jiang, H. (2022). Identification of prefrontal cortex and amygdala expressed genes associated with Sevoflurane anesthesia on non-human primate. *Frontiers in Integrative Neuroscience*, *16*, 857349.

Gassó, P., Sánchez-Gistau, V., Mas, S., Sugranyes, G., Rodríguez, N., Boloc, D., de la Serna, E., Romero, S., Moreno, D., Moreno, C., Díaz-Caneja, C. M., Lafuente, A., & Castro-Fornieles, J. (2016). Association of CACNA1C and SYNE1 in offspring of patients with psychiatric disorders. *Psychiatry Research*, *245*, 427–435.

Kodama, M., Satoh, Y., Otsubo, Y., Araki, Y., Yonamine, R., Masui, K., & Kazama, T. (2011). Neonatal desflurane exposure induces more robust neuroapoptosis than do isoflurane and sevoflurane and impairs working memory. *Anesthesiology*, *115*, 979–991.

Leussis, M. P., Berry-Scott, E. M., Saito, M., Jhuang, H., de Haan, G., Alkan, O., Luce, C. J., Madison, J. M., Sklar, P., Serre, T., Root, D. E., & Petryshen, T. L. (2013). The ANK3 bipolar disorder gene regulates psychiatric-related behaviors that are modulated by lithium and stress. *Biological Psychiatry*, *73*, 683–690.

Liang, L., Zeng, T., Zhao, Y., Lu, R., Guo, B., Xie, R., Tang, W., Zhang, L., Mao, Z., Yang, X., Wu, S., Wang, Y., & Zhang, H. (2021). Melatonin pretreatment alleviates the long-term synaptic toxicity and dysmyelination induced by neonatal Sevoflurane exposure via MT1 receptor-mediated Wnt signaling modulation. *Journal of Pineal Research*, *71*, e12771.

Mar, J. C., Matigian, N. A., Mackay-Sim, A., Mellick, G. D., Sue, C. M., Silburn, P. A., McGrath, J. J., Quackenbush, J., & Wells, C. A. (2011). Variance of gene expression identifies altered network constraints in neurological disease. *PLoS Genetics*, *7*, e1002207.

McCann, M. E., de Graaff, J. C., Dorris, L., Disma, N., Withington, D., Bell, G., Grobler, A., Stargatt, R., Hunt, R. W., Sheppard, S. J., Marmor, J., Giribaldi, G., Bellinger, D. C., Hartmann, P. L., Hardy, P., Frawley, G., Izzo, F., von Ungern Sternberg, B. S., Lynn, A., … Davidson, A. J. (2019). Neurodevelopmental outcome at 5 years of age after general anaesthesia or awake-regional anaesthesia in infancy (GAS): An international, multicentre, randomised, controlled equivalence trial. *Lancet*, *393*, 664–677.

Miller, E. K., Freedman, D. J., & Wallis, J. D. (2002). The prefrontal cortex: Categories, concepts and cognition. *Philosophical Transactions of the Royal Society of London. Series B, Biological Sciences*, *357*, 1123–1136.

Morgunova, A., Pokhvisneva, I., Nolvi, S., Entringer, S., Wadhwa, P., Gilmore, J., Styner, M., Buss, C., Sassi, R. B., Hall, G. B. C., O'Donnell, K. J., Meaney, M. J., Silveira, P. P., & Flores, C. A. (2020). DCC gene network in the prefrontal cortex is associated with total brain volume in childhood. *Journal of Psychiatry & Neuroscience*, *46*, E154–e163.

Nudel, R., Zetterberg, R., Hemager, N., Christiani, C. A. J., Ohland, J., Burton, B. K., Greve, A. N., Spang, K. S., Ellersgaard, D., Gantriis, D. L., Bybjerg-Grauholm, J., Plessen, K. J., Jepsen, J. R. M., Thorup, A. A. E., Werge, T., Mors, O., & Nordentoft, M. (2022). A family-based study of genetic and epigenetic effects across multiple neurocognitive, motor, social-cognitive and social-behavioral functions. *Behavioral and Brain Functions*, *18*, 14.

Paus, T., Keshavan, M., & Giedd, J. N. (2008). Why do many psychiatric disorders emerge during adolescence? *Nature Reviews. Neuroscience*, *9*, 947–957.

Rabbitts, J. A., Groenewald, C. B., Moriarty, J. P., & Flick, R. (2010). Epidemiology of ambulatory anesthesia for children in the United States: 2006 and 1996. *Anesthesia and Analgesia*, *111*, 1011–1015.

Shi, Y., Hu, D., Rodgers, E. L., Katusic, S. K., Gleich, S. J., Hanson, A. C., Schroeder, D. R., Flick, R. P., & Warner, D. O. (2018). Epidemiology of general anesthesia prior to age 3 in a population-based birth cohort. *Paediatric Anaesthesia*, *28*, 513–519.

Shipp, S. (2007). Structure and function of the cerebral cortex. *Current Biology*, *17*, R443–R449.

Sobieski, C., Fitzpatrick, M. J., & Mennerick, S. J. (2017). Differential presynaptic ATP supply for basal and high-demand transmission. *The Journal of Neuroscience*, *37*, 1888–1899.

Sokolova, E., Oerlemans, A. M., Rommelse, N. N., Groot, P., Hartman, C. A., Glennon, J. C., Claassen, T., Heskes, T., & Buitelaar, J. K. (2017).

A causal and mediation analysis of the comorbidity between attention deficit hyperactivity disorder (ADHD) and autism Spectrum disorder (ASD). *Journal of Autism and Developmental Disorders*, *47*, 1595–1604.

Song, S., Zhao, W., Ji, Y., Huang, Q., Li, Y., Chen, S., Yang, J., & Jin, X. (2023). SHANK2 protein contributes to sevoflurane-induced developmental neurotoxicity and cognitive dysfunction in C57BL/6 male mice. *Anesthesiology and Perioperative Science*, *1*, 2.

Song, S. Y., Meng, X. W., Xia, Z., Liu, H., Zhang, J., Chen, Q. C., Liu, H. Y., Ji, F. H., & Peng, K. (2019). Cognitive impairment and transcriptomic profile in hippocampus of young mice after multiple neonatal exposures to sevoflurane. *Aging (Albany NY)*, *11*, 8386–8417.

Song, S. Y., Peng, K., Meng, X. W., Shan, X. S., Chen, Q. C., Zhao, W. M., Shen, B., Qiu, H., Liu, H., Liu, H. Y., & Ji, F. H. (2023). Single-nucleus atlas of Sevoflurane-induced hippocampal cell type- and sex-specific effects during development in mice. *Anesthesiology*, *138*, 477–495.

Sun, M., Xie, Z., Zhang, J., & Leng, Y. (2022). Mechanistic insight into sevoflurane-associated developmental neurotoxicity. *Cell Biology and Toxicology*, *38*, 927–943.

Warner, D. O., Zaccariello, M. J., Katusic, S. K., Schroeder, D. R., Hanson, A. C., Schulte, P. J., Buenvenida, S. L., Gleich, S. J., Wilder, R. T., Sprung, J., Hu, D., Voigt, R. G., Paule, M. G., Chelonis, J. J., & Flick, R. P. (2018). Neuropsychological and behavioral outcomes after exposure of young children to procedures requiring general anesthesia: The Mayo anesthesia safety in kids (MASK) study. *Anesthesiology*, *129*, 89–105.

Wu, Z., Xue, H., Gao, Q., & Zhao, P. (2020). Effects of early postnatal sevoflurane exposure on oligodendrocyte maturation and myelination in cerebral white matter of the rat. *Biomedicine & Pharmacotherapy*, *131*, 110733.

Xu, L., Xu, Q., Dai, S., Jiao, C., Tang, Y., Xie, J., Wu, H., & Chen, X. (2021). lncRNA Xist regulates sevoflurane-induced social and emotional impairment by modulating miR-98-5p/EDEM1 signaling axis in neonatal mice. *Molecular Therapy - Nucleic Acids*, *24*, 939–950.

Xu, X., Tian, X., & Wang, G. (2018). Sevoflurane reduced functional connectivity of excitatory neurons in prefrontal cortex during working memory performance of aged rats. *Biomedicine & Pharmacotherapy*, *106*, 1258–1266.

Zeisel, A., Munoz-Manchado, A. B., Codeluppi, S., Lonnerberg, P., La Manno, G., Jureus, A., Marques, S., Munguba, H., He, L., Betsholtz, C., Rolny, C., Castelo-Branco, G., Hjerling-Leffler, J., & Linnarsson, S. (2015). Brain structure. Cell types in the mouse cortex and hippocampus revealed by single-cell RNA-seq. *Science*, *347*, 1138–1142.

Zhang, L., Cheng, Y., Xue, Z., Li, J., Wu, N., Yan, J., Wang, J., Wang, C., Chen, W., Zhou, T., Qiu, Z., & Jiang, H. (2022). Sevoflurane impairs m6A-mediated mRNA translation and leads to fine motor and cognitive deficits. *Cell Biology and Toxicology*, *38*, 347–369.

Zheng, F., Liu, G., Dang, T., Chen, Q., An, Y., Wu, M., Kong, X., Qiu, Z., & Wu, B. L. (2021). GABA signaling pathway-associated gene PLCL1 rare variants may be associated with autism spectrum disorders. *Neuroscience Bulletin*, *37*, 1240–1245.

SUPPORTING INFORMATION

Additional supporting information can be found online in the Supporting Information section at the end of this article.

How to cite this article: Zhao, B.-J., Song, S.-Y., Zhao, W.-M., Xu, H.-B., Peng, K., Shan, X.-S., Chen, Q.-C., Liu, H., Liu, H.-Y., & Ji, F.-H. (2024). The effect of sevoflurane exposure on cell-type-specific changes in the prefrontal cortex in young mice. *Journal of Neurochemistry*, *00*, 1–17. https://doi.org/10.1111/jnc.16068